

Quantum corrections to a spin-orbit coupled Bose-Einstein Condensate

Long Liang^{1,2} and Päivi Törmä¹

1, Department of Applied Physics, Aalto University School of Science, FI-00076 Aalto, Finland
2, Computational Physics Laboratory, Physics Unit, Faculty of Engineering and Natural Sciences, Tampere University, P.O. Box 692, FI-33014 Tampere, Finland

We study systematically the quantum corrections to a weakly interacting Bose-Einstein condensate with spin-orbit coupling. We show that quantum fluctuations, enhanced by the spin-orbit coupling, can dramatically modify the mean-field properties such as the superfluid density, spin polarizability, and sound velocity. We also calculate the Beliaev and Landau damping rates and find that the Landau process dominates the quasiparticle decay even at low temperature. Our results show that spin-orbit coupled bosons represent a promising system for exploring beyond mean-field physics.

The spin-orbit coupling, arising due to the interaction of a particle's spin with its motion in an electric field plays a crucial role in various branches of physics, including topological insulators [1, 2], topological semimetals [3, 4], and Majorana fermions [5]. In bosonic systems, the interplay of the interparticle interaction and spin-orbit coupling gives rise to exotic Bose-Einstein condensates which have been investigated in a rich variety of systems, including magnons [6–8], excitons [9–12], exciton-polaritons [13–18], and ultracold atoms [19–22].

For a weakly interacting Bose-Einstein condensate, the mean-field theory provides a reliable description of various physical properties [23]. To reveal beyond mean-field effects, one method is to reach the strongly interacting regime, which can be achieved in exciton-polaritons because of the strong coupling between the exciton and photon [13, 24–27], and for ultracold atoms strong interactions are accessible by means of Feshbach resonances [28–30]. However, strong interactions reduce the lifetime of Bose-Einstein condensates significantly. Another method is to fine tune the interaction parameters such that the mean-field interactions almost cancel out [31–34], making the quantum fluctuations unmasked. The spin-orbit coupling provides an alternative way to enhance interaction effects due to the increased density of states [35]. However, only a handful of theoretical studies have addressed the beyond mean-field effects [36–40], and a thorough analysis of the quantum fluctuations in spin-orbit coupled bosonic systems is still lacking.

In this Letter, we systematically investigate the quantum corrections to a spin-orbit coupled Bose-Einstein condensate. We study a model system that is simple and general, potentially realizable in various platforms and already implemented with ultracold atom experiments [19–21]. The model shows three novel condensation phases [19, 41], namely the stripe, plane wave, and zero momentum phases. To demonstrate the interplay between interaction and spin-orbit coupling, we focus on the zero momentum phase, which is the simplest case capturing the essential physics of spin-orbit coupling and interactions.

Most importantly, we show that near the phase bound-

ary between the plane wave and zero momentum phases, quantum fluctuations dramatically modify the mean-field scaling behavior of the sound velocity with respect to the transverse field. The qualitative change of the sound velocity can be detected in current cold atom experiments. Contrary to the mean-field predictions [42–45], we also find that at the phase transition point, the superfluid density becomes nonzero and the spin polarizability remains finite, which seems to be consistent with a recent experiment [20]. Finally, we obtain an analytical result for the Landau decay rate of phonons at low temperature. Unlike the Beliaev decay predicted in [40], the Landau damping is not suppressed in the direction of spin-orbit coupling, making it the dominant mechanism for the quasiparticle decay.

The model system. We consider a generic model of a spin-1/2 Bose gas with spin-orbit coupling, described by the single particle Hamiltonian (we set $\hbar = m = 1$)

$$h_0 = \frac{(p_x - k_0 \sigma_z)^2 + p_y^2 + p_z^2}{2} + \frac{\Omega}{2} \sigma_x, \quad (1)$$

where σ_i with $i = x, y, z$ are the 2×2 Pauli matrices. The one dimensional spin-orbit coupling, characterized by k_0 , appears in many realistic systems, including ultracold gases [19–21, 46, 47] and semiconducting nanowires [48–50]. The model applies to several systems but to compare with experiments, we consider the cold atom setup where k_0 is given by the momentum transfer from the two Raman laser beams and Ω is the Rabi frequency of the Raman beams. The interaction between the particles can be written as

$$H_{\text{int}} = \frac{1}{2} \sum_{\sigma\sigma'} \int d^3\mathbf{r} g_{\sigma\sigma'} n_{\sigma}(\mathbf{r}) n_{\sigma'}(\mathbf{r}), \quad (2)$$

where n_{σ} is the density of particles with spin $\sigma = \uparrow, \downarrow$, and $g_{\sigma\sigma'} = 4\pi a_{\sigma\sigma'}$ are the interaction strengths in different spin channels, with $a_{\sigma\sigma'}$ being the corresponding s -wave scattering lengths in case of ultracold quantum gases. In the following we assume $g_{\uparrow\uparrow} = g_{\downarrow\downarrow} \equiv g$ and $g_{\uparrow\downarrow} \equiv g'$, and correspondingly, $a_{\uparrow\uparrow} = a_{\downarrow\downarrow} \equiv a$ and $a_{\uparrow\downarrow} \equiv a'$. It is convenient to define interaction parameters $G_1 = g + \rho$ and $G_2 = g - \rho$ with $g_{\pm} = (g \pm g')/2$ and $\rho = N/V$

being the total particle density. In recent experiments [19–21], ^{87}Rb atoms are employed and the interaction is almost $SU(2)$ invariant, with $G_2/G_1 \approx 10^{-3}$. The typical interaction parameter is $G_1 \approx 0.24k_0^2$ with the peak density $\rho \approx 0.57k_0^3$ [20]. The dimensionless parameter $\sqrt{a^3\rho} \approx 0.004$ is small, ensuring that the condensate is in the weakly interacting regime and the perturbation calculations are controlled.

The mean-field phase diagram of this model has been extensively investigated, for a review see [35]. For small Rabi frequency, the condensate wave function is a superposition of two plane waves with different momenta, characterizing the stripe phase with density modulations in the ground state. In this phase, both the translational and $U(1)$ symmetries are broken, and therefore there are two branches of gapless excitations. Increasing the Rabi frequency Ω , the system enters the plane wave phase, in which the bosons condense in a single plane wave state. There is only one branch of gapless excitations in this phase and the energy dispersion contains a roton minimum at finite momentum. Further increasing the Rabi frequency such that $\Omega > 2k_0^2 - 2G_2$, the system enters the zero momentum phase, where the roton minimum disappears and the phonon excitation spectrum resembles that of a Bose-Einstein condensate without spin-orbit coupling. To reveal the essential effect of interactions, we focus on the simplest zero momentum phase to reduce the effect of nontrivial mean-field energy dispersions in the plane wave and stripe phases.

Method. The ground state wave function for the zero momentum phase is described by a spinor $\psi = \sqrt{\rho/2}[1, -1]^T$. To characterize excitations on top of the condensate, we introduce phase and number fluctuations, and write the spinor field as

$$\psi = \frac{e^{i\phi}}{\sqrt{2}} \begin{bmatrix} \sqrt{\rho + \zeta_1} e^{i\varphi} \\ -\sqrt{\rho + \zeta_2} e^{-i\varphi} \end{bmatrix}, \quad (3)$$

where ϕ is the total and φ is the relative phase fluctuations of the condensate, and ζ_1 and ζ_2 are the density fluctuations for spin up and spin down particles, respectively.

We use the imaginary time path integral formalism. The Lagrangian density is obtained through the Hamiltonian as

$$\mathcal{L} = \psi^\dagger(\partial_\tau + h_0 - \mu)\psi + \frac{g_+}{2}(\psi^\dagger\psi)^2 + \frac{g_-}{2}(\psi^\dagger\sigma_z\psi)^2, \quad (4)$$

with μ being the chemical potential. It is convenient to introduce the density and spin fluctuations, $\zeta_+ = (\zeta_1 + \zeta_2)/2$ and $\zeta_- = (\zeta_1 - \zeta_2)/2$, which are conjugate to ϕ and φ , respectively. We then expand \mathcal{L} in terms of the new variables, and up to the second order, we get the mean-field Lagrangian density

$$\mathcal{L}_{\text{mf}} = \left(G_1 + \frac{k_0^2 - \Omega}{2} - \mu \right) \zeta_+ - \mu\rho + \frac{g_+\rho^2}{2} + \frac{1}{2}[\phi, \zeta_+, \varphi, \zeta_-] \mathcal{G}_0^{-1}[\phi, \zeta_+, \varphi, \zeta_-]^T, \quad (5)$$

where the mean-field Green's function in the momentum and frequency representation is

$$\mathcal{G}_0^{-1}(i\omega_n, \mathbf{q}) = \begin{bmatrix} \mathcal{A}(\mathbf{q}) & -\omega_n & 0 & -ik_0q_x \\ \omega_n & \mathcal{B}(\mathbf{q}) & ik_0q_x & 0 \\ 0 & -ik_0q_x & \mathcal{C}(\mathbf{q}) & -\omega_n \\ ik_0q_x & 0 & \omega_n & \mathcal{D}(\mathbf{q}) \end{bmatrix}, \quad (6)$$

here $\omega_n = 2\pi nT$ is the Matsubara frequency (we set $k_B = 1$), $\mathcal{A}(\mathbf{q}) = \rho\mathbf{q}^2$, $\mathcal{B}(\mathbf{q}) = \mathbf{q}^2/(4\rho) + g_+$, $\mathcal{C}(\mathbf{q}) = \rho\mathbf{q}^2 + 2\Omega\rho$, and $\mathcal{D}(\mathbf{q}) = \mathbf{q}^2/(4\rho) + g_- + \Omega/(2\rho)$. The chemical potential is determined by requiring $\langle \zeta_+ \rangle = 0$, and at the mean-field level we find $\mu = G_1 + (k_0^2 - \Omega)/2$, so the first order term of ζ_+ vanishes and the mean-field Lagrangian density is quadratic.

Mean-field results. Before studying the beyond mean-field corrections, we present some mean-field results which are readily obtained from the mean-field Green's function.

The mean-field excitation energy is determined by $\det \mathcal{G}_0^{-1} = 0$. In the low momentum limit, we find the gapless phonon dispersion to be

$$\varepsilon_{\text{ph}} = c_0 \sqrt{q^2 - \frac{2k_0^2 q_x^2}{\Omega + 2G_2}} = c_0 q \sqrt{1 - \frac{2k_0^2 \cos^2 \theta}{\Omega + 2G_2}} \equiv c_\theta q, \quad (7)$$

where $c_0 = \sqrt{G_1}$ and c_θ is the sound velocity which depends on the angle θ between the directions of the momentum \mathbf{q} and the x axis. The mean-field sound velocities c_y and c_z are the same as the usual Bogoliubov sound velocity c_0 . An intriguing feature is that the mean-field sound velocity in the x direction, c_x , vanishes at the phase transition point between the plane wave and zero momentum phases. Besides the gapless phononic mode, there also exists a gapped mode which is dominated by spin excitation, with the mean-field gap given by $\Delta_0 = \sqrt{\Omega(\Omega + 2G_2)}$.

The density and spin response functions are given by the Green's functions $\mathcal{G}_{\zeta_+\zeta_+}$ and $\mathcal{G}_{\zeta_-\zeta_-}$, respectively. From the spin response function, the spin polarizability [42, 43] can be obtained, and at the mean-field level, we get

$$\chi_M = \mathcal{G}_{0,\zeta_-\zeta_-}(q_x \rightarrow 0)/\rho = \frac{2}{\Omega + 2G_2 - 2k_0^2}, \quad (8)$$

which diverges at the phase transition point.

An important quantity characterizing superfluidity is the superfluid density, which governs the total phase fluctuations. To get the superfluid density, we integrate out the φ , ζ_- and ζ_+ fields and obtain an effective theory of ϕ (see Supplemental Material). In the low energy and long wave length limit, we find

$$\mathcal{L}_{\text{eff}} = (K\omega_n^2 + \rho_i q_i^2)|\phi|^2, \quad (9)$$

where K is the zero momentum static density response function with its mean-field value being $1/g_+$, and $\rho_y = \rho_z = \rho$, $\rho_x = \rho[1 - 2k_0^2/(\Omega + 2G_2)]$ are the mean-field

superfluid densities. From the effective Lagrangian, we see that the sound velocity is related to the superfluid density through $c_i = \sqrt{K^{-1}\rho_i}$.

In [44], the superfluid density ρ_x is calculated from the current-current correlation function, which can be written in terms of the transverse spin polarization $\langle\sigma_x\rangle$ and the excitation gap Δ as $\rho_x = \rho(1 + 2k_0^2\Omega\langle\sigma_x\rangle/\Delta^2)$. Substituting the mean-field values $\Delta = \Delta_0$ and $\langle\sigma_x\rangle = -1$,

$$\mathcal{L}_{\text{fluct}} = \frac{\zeta_+}{2}[(\nabla\phi)^2 + (\nabla\varphi)^2] + \zeta_- \nabla\phi\nabla\varphi - \frac{\Omega\rho}{3}\varphi^4 + \Omega\zeta_+\varphi^2 - \frac{\Omega}{2\rho}\zeta_-^2\varphi^2 - \frac{\Omega}{2}\left(\frac{\zeta_+\zeta_-^2}{2\rho^2} - \frac{\zeta_-^2\zeta_+^2}{2\rho^3} - \frac{\zeta_-^4}{8\rho^3}\right),$$

$$- \frac{\zeta_+[(\nabla\zeta_+)^2 + (\nabla\zeta_-)^2]}{8\rho^2} - \frac{\zeta_- \nabla\zeta_+ \nabla\zeta_-}{4\rho^2} + \frac{(\zeta_+^2 + \zeta_-^2)[(\nabla\zeta_+)^2 + (\nabla\zeta_-)^2] + \nabla\zeta_+^2 \nabla\zeta_-^2}{8\rho^3}. \quad (10)$$

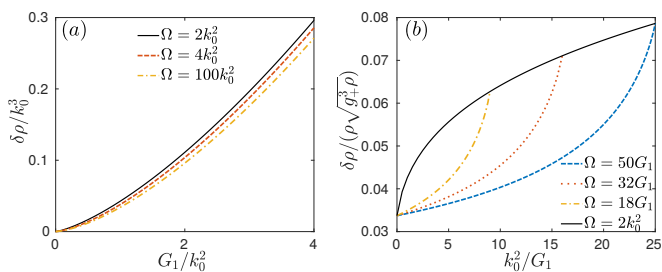


FIG. 1. The quantum depletion as a function of the interaction (a) and spin-orbit coupling (b) for different Raman fields Ω . The solid lines correspond to the phase transition between the zero momentum and plane wave phases.

Without the spin-orbit coupling, the one-loop corrections can be calculated analytically, and the results are given in Supplemental Material. In the main text we focus on the more interesting situation with nonzero spin-orbit coupling and calculate the one-loop corrections numerically. Since the parameter G_2 is small, we take it to be zero unless otherwise mentioned.

Quantum depletion. Due to the quantum fluctuations, the condensate is depleted by a fraction of the total density. Up to the lowest order, the quantum depletion is given by (see Supplemental Material) $\delta\rho = \rho(\langle\phi^2\rangle + \langle\varphi^2\rangle) + (\langle\zeta_+^2\rangle + \langle\zeta_-^2\rangle)/(4\rho)$. Fig. 1 shows the quantum depletion as a function of the interaction strength and spin-orbit coupling. The quantum depletion increases with the interaction strength. We find that it also increases with the spin-orbit coupling strength, which is consistent with previous results [36, 37]. As Fig. 1 shows, the quantum depletion takes the largest value at the phase transition point, $\Omega = 2k_0^2$.

Ground state energy and chemical potential. We study the correction to the mean-field energy density, which is known as the Lee-Huang-Yang (LHY) correction [51] \mathcal{E}_{LHY} , and can be viewed as the zero point energy of the excitations [52]. With increasing k_0 , the

we obtain from this the same result as given by the effective theory method above. Note that if the gap becomes larger or σ_x is not fully polarized, the superfluid density ρ_x will increase.

Beyond mean-field corrections. To study the lowest order (one-loop) beyond mean-field corrections, we expand the Lagrangian density up to the fourth order of the fields,

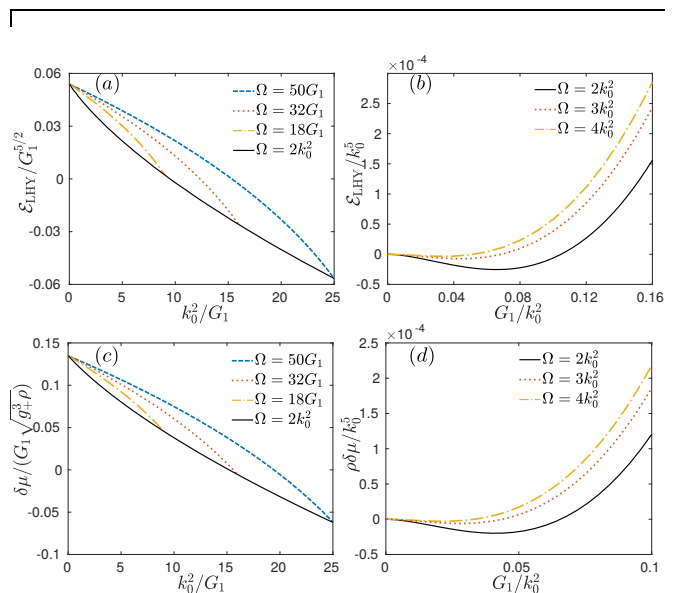


FIG. 2. The LHY correction [(a) and (b)] and the chemical potential shift [(c) and (d)] as a function of the spin-orbit coupling and interaction for different Raman fields Ω . The value $\Omega = 2k_0^2$ corresponds to the phase transition.

phonon mode softens, and therefore the zero point energy decreases and the LHY correction reaches its minimum value at the phase boundary. Fig. 2 (a) shows this behavior clearly. Remarkably, we find that \mathcal{E}_{LHY} becomes negative for large enough spin-orbit coupling. This leads to a non-monotonic dependence of \mathcal{E}_{LHY} on G_1 : If we fix k_0 and increase G_1 from zero, then for small G_1 (large k_0^2/G_1), the LHY correction decreases from zero to negative; increasing G_1 further, the LHY correction will increase since it becomes positive for small k_0^2/G_1 . The non-monotonic behavior of \mathcal{E}_{LHY} is most clearly seen at the phase transition point, see Fig. 2 (b).

We then calculate the correction to the chemical potential, which is given by the tadpole diagrams shown in Supplemental Material. The numerical results of $\delta\mu$ are

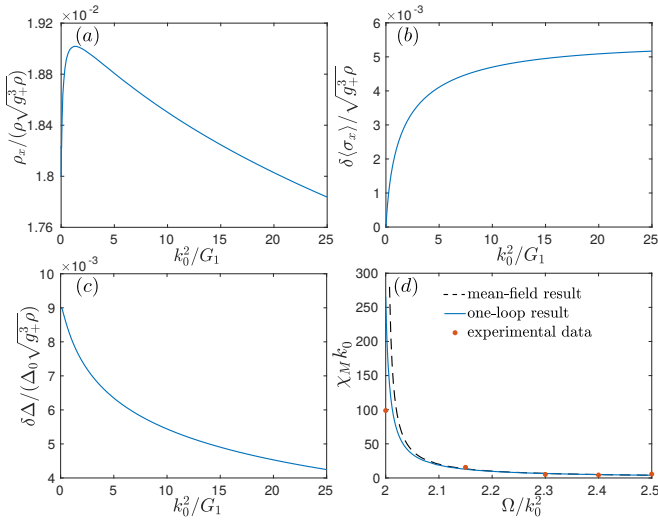


FIG. 3. The superfluid density (a), the deviation of the transverse spin polarization (b), and the spin excitation gap (c) at the phase transition point. The spin polarizability as a function of Ω (d). The experimental data are taken from [20]. To simulate the experiment, we use $k_0^2 = 4.2G_1$, $\sqrt{g_+^3 \rho} = 0.2$, and $G_2/G_1 = 10^{-3}$ in the one-loop calculation.

shown in Figs. 2 (c) and (d). As the LHY correction, the chemical potential shift decreases with increasing of k_0 and depends non-monotonically on G_1 . This is expected, because the chemical potential shift can also be obtained as the first order derivative of the LHY energy with respect to the density.

Superfluid density and spin polarizability. To get the correction to the superfluid density, we first calculate the one-loop self-energy and then integrate out the massive fields φ , ζ_- and ζ_+ to get the effective Lagrangian of the total phase fluctuations. The superfluid density in the x direction is found to be

$$\rho_x = \rho \left[1 - \frac{2k_0^2}{\Omega + 2G_2 - 2\rho \Sigma_{\zeta_- \zeta_-}(0)} \right], \quad (11)$$

where $\Sigma_{\zeta_- \zeta_-}(0)$ is the self-energy at zero frequency and momentum. There is no correction to ρ_y and ρ_z at zero temperature, consistent with the general result of superfluid density in Galilean invariant superfluids [53].

Importantly, Fig. 3 (a) shows that contrary to the previous predictions [44, 45], the superfluid density remains nonzero at the phase transition point. Physically, this can be explained by the decrease of the transverse polarization $\langle \sigma_x \rangle$ and the increase of the spin gap Δ .

Because of the spin-orbit coupling, the spin of excited particles is not perfectly along the x direction, and therefore the magnitude of the transverse spin polarization is reduced. Up to the lowest order, the deviation of spin polarization is (see Supplemental Material) $\delta \langle \sigma_x \rangle = 2\langle \varphi^2 \rangle + \langle \zeta_-^2 \rangle / (2\rho^2)$. We plot the numerical result of $\delta \langle \sigma_x \rangle$ in Fig. 3 (b). Another quantity that determines

ρ_x is the excitation gap. We obtain from the one-loop self-energy the correction to the mean-field gap and find it is positive, see Fig. 3 (c). Combining the behavior of $\delta \langle \sigma_x \rangle$ and Δ , the non-monotonic dependence of ρ_x on k_0^2 can be explained: The superfluid density increases with increasing $\delta \langle \sigma_x \rangle$ and Δ , and with increasing k_0 , $\delta \langle \sigma_x \rangle$ increases but Δ decreases. As a result, the superfluid weight first increases and then decreases with increasing the spin-orbit coupling strength.

The self-energy $\Sigma_{\zeta_- \zeta_-}(0)$ also gives correction to the spin polarizability,

$$\chi_M = \frac{2}{\Omega + 2G_2 - 2k_0^2 - 2\rho \Sigma_{\zeta_- \zeta_-}(0)}. \quad (12)$$

Importantly, in contrast to the mean-field result [42, 43], χ_M becomes finite at the phase transition point. The spin polarizability has been measured [20], and it seems that our one-loop result agrees better with the experimental data than the mean-field theory, see Fig. 3 (d). However, the current experimental data cannot lead to a decisive conclusion and future experiments are required to verify our prediction.

Sound velocity and damping rate. We have shown that due to quantum fluctuations, the superfluid density ρ_x at the phase transition point becomes nonzero. Although its value is small, it has a significant effect on the phonon dispersion through the correction to the sound velocity, $c_x = \sqrt{K^{-1} \rho_x}$. Using the one-loop results for the static density response K^{-1} and the superfluid density ρ_x , we obtain the quantum corrected c_x , see Fig. 4.

A direct result of nonzero ρ_x is that c_x also becomes nonzero at the phase transition point, which is consistent with the result in [54]. Most interestingly, we discover that quantum fluctuations qualitatively modify the scaling behavior of the sound velocity near the phase transition point. Close to the phase transition point, the mean-field theory predicts that the sound velocity increases linearly with increasing $\sqrt{\delta \Omega}$, where $\delta \Omega = \Omega - 2k_0^2$. This mean-field behavior breaks down near the phase boundary as clearly shown in Fig. 4. For typical experimental parameters [19–21], the deviation from the linear scaling becomes significant when $\sqrt{\delta \Omega}/k_0 < 0.1$. The sound velocity has been measured [21], but the parameters are not close enough to the phase transition point. However, our prediction should be observable with current experimental methods.

Finally, we calculate the damping rate of phonons, for details see Supplemental Material. At zero temperature, the damping is due to the Beliaev process [55], i.e., an excitation decays into two with lower energy. In the small momentum limit ($q_y, q_z \ll \sqrt{G_1}$ and $q_x \ll \sqrt{\Omega - 2k_0^2}$), we find

$$\gamma_B = \frac{3q^5}{640\pi\rho} \left[1 - \frac{2\Omega k_0^2 \cos^2 \theta}{(\Omega + 2G_2)^2} \right]^2 \sqrt{1 + \frac{2k_0^2 \sin^2 \theta}{\Omega + 2G_2 - 2k_0^2}}, \quad (13)$$

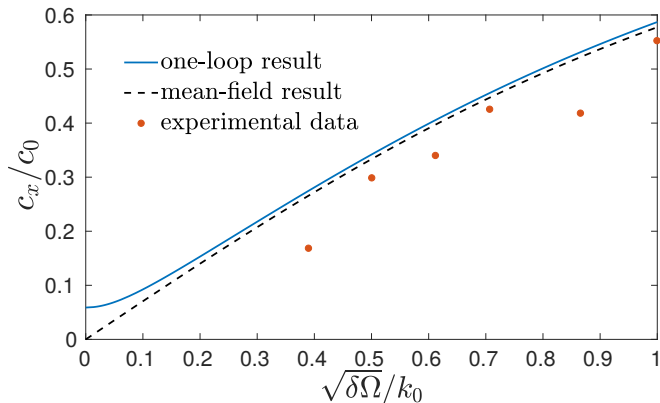


FIG. 4. The sound velocity c_x along the x direction ($c_0 = \sqrt{G_1}$). Here $\delta\Omega = \Omega - 2k_0^2$. The experimental data are taken from [21], and the parameters we use to calculate the one-loop result are $k_0^2 = 5.2G_1$, $\sqrt{g_+^3\rho} = 0.18$, and $G_2/G_1 = 10^{-3}$, which correspond to the experiment in [21].

which coincides with the result obtained in [40]. The Beliaev damping is strongly suppressed along the direction of the spin-orbit coupling.

At finite temperature, the Landau damping [56] arises because the phonon couples to thermal excitations. The Landau damping is experimentally more relevant since it is responsible for damping in trapped Bose gases [57–59]. In the low temperature and small momentum limit ($c_\theta q \ll T \ll \Omega - 2k_0^2$), we obtain

$$\gamma_L = \frac{3\pi^3 q T^4}{40\rho c_\theta^4} \left[1 - \frac{2\Omega k_0^2 \cos^2 \theta}{(\Omega + 2G_2)^2} \right]^2 \sqrt{1 + \frac{2k_0^2 \sin^2 \theta}{\Omega + 2G_2 - 2k_0^2}}. \quad (14)$$

Because of the extra c_θ dependence, the Landau damping rate, unlike the Beliaev decay, is not suppressed in the direction of spin-orbit coupling, which means that the Landau process is the dominant damping mechanism even for uniform systems at very low temperature.

Conclusion. We calculate systematically the one-loop corrections to a spin-orbit coupled Bose-Einstein condensate. We find that quantum fluctuations cause significant changes in the ground state, superfluid density, spin polarizability, sound velocity, and damping rate. The maximum of the quantum depletion and the minimum of the LHY correction are found at the transition point between the zero momentum and plane wave phases. At the transition, the superfluid density and the spin polarizability show qualitatively different behavior compared to the mean-field prediction: they remain finite, consistent with an experimental measurement of the spin polarizability [20]. We identify Landau damping as the dominant mechanism of quasiparticle decay. Our results show that the spin-orbit coupling leads to, even for moderate interactions, quantum fluctuations strong enough to significantly, and qualitatively, modify the ground state prop-

erties of a macroscopic quantum state such as a Bose-Einstein condensate. The results can be readily tested in ultracold quantum gases, and in the future, in spin-orbit coupled Bose-Einstein condensates realized in other systems.

Acknowledgements. This work was supported by the Academy of Finland under Projects No. 303351, No. 307419, No. 318987, and by the European Research Council (ERC-2013-AdG-340748-CODE). L.L. would like to acknowledge the Aalto Centre for Quantum Engineering for support.

-
- [1] M. Z. Hasan and C. L. Kane, “Colloquium: Topological insulators,” *Rev. Mod. Phys.* **82**, 3045 (2010).
 - [2] X.-L. Qi and S.-C. Zhang, “Topological insulators and superconductors,” *Rev. Mod. Phys.* **83**, 1057 (2011).
 - [3] B. Yan and C. Felser, “Topological materials: Weyl semimetals,” *Annu. Rev. Condens. Matter Phys.* **8**, 337 (2017).
 - [4] N. P. Armitage, E. J. Mele, and A. Vishwanath, “Weyl and Dirac semimetals in three-dimensional solids,” *Rev. Mod. Phys.* **90**, 015001 (2018).
 - [5] S. R. Elliott and M. Franz, “Colloquium: Majorana fermions in nuclear, particle, and solid-state physics,” *Rev. Mod. Phys.* **87**, 137 (2015).
 - [6] Ch. Rüegg, N. Cavadini, A. Furrer, H.-U. Güdel, K. Krämer, H. Mutka, A. Wildes, K. Habicht, and P. Vorderwisch, “Bose-Einstein condensation of the triplet states in the magnetic insulator TlCuCl_3 ,” *Nature* **423**, 62 (2003).
 - [7] J. Sirker, A. Weiße, and O. P. Sushkov, “Consequences of spin-orbit coupling for the Bose-Einstein condensation of magnons,” *EPL* **68**, 275 (2004).
 - [8] S. O. Demokritov, V. E. Demidov, O. Dzyapko, G. A. Melkov, A. A. Serga, B. Hillebrands, and A. N. Slavin, “Bose-Einstein condensation of quasi-equilibrium magnons at room temperature under pumping,” *Nature* **443**, 430 (2006).
 - [9] T. Hakioglu and M. Şahin, “Excitonic condensation under spin-orbit coupling and BEC-BCS crossover,” *Phys. Rev. Lett.* **98**, 166405 (2007).
 - [10] M. A. Can and T. Hakioglu, “Unconventional pairing in excitonic condensates under spin-orbit coupling,” *Phys. Rev. Lett.* **103**, 086404 (2009).
 - [11] A. A. High, J. R. Leonard, A. T. Hammack, M. M. Fogler, L. V. Butov, A. V. Kavokin, K. L. Campman, and A. C. Gossard, “Spontaneous coherence in a cold exciton gas,” *Nature (London)* **483**, 584 (2012).
 - [12] A. A. High, A. T. Hammack, J. R. Leonard, Sen Yang, L. V. Butov, T. Ostatnický, M. Vladimirova, A. V. Kavokin, T. C. H. Liew, K. L. Campman, and A. C. Gossard, “Spin currents in a coherent exciton gas,” *Phys. Rev. Lett.* **110**, 246403 (2013).
 - [13] I. Carusotto and C. Ciuti, “Quantum fluids of light,” *Rev. Mod. Phys.* **85**, 299 (2013).
 - [14] T. Byrnes, N. Y. Kim, and Y. Yamamoto, “Exciton-polariton condensates,” *Nat. Phys.* **10**, 803 (2014).
 - [15] V. G. Sala, D. D. Solnyshkov, I. Carusotto, T. Jacqmin, A. Lemaître, H. Terças, A. Nalitov, M. Abbarchi, E. Ga-

- lopin, I. Sagnes, J. Bloch, G. Malpuech, and A. Amo, “Spin-orbit coupling for photons and polaritons in microstructures,” *Phys. Rev. X* **5**, 011034 (2015).
- [16] C. E. Whittaker, E. Cancellieri, P. M. Walker, D. R. Gulevich, H. Schomerus, D. Vaitiekus, B. Royall, D. M. Whittaker, E. Clarke, I. V. Iorsh, I. A. Shelykh, M. S. Skolnick, and D. N. Krizhanovskii, “Exciton polaritons in a two-dimensional Lieb lattice with spin-orbit coupling,” *Phys. Rev. Lett.* **120**, 097401 (2018).
- [17] S. Klembt, T. H. Harder, O. A. Egorov, K. Winkler, H. Suchomel, J. Beierlein, M. Emmerling, C. Schneider, and S. Höfling, “Polariton condensation in S- and P-flatbands in a two-dimensional Lieb lattice,” *Appl. Phys. Lett.* **111**, 231102 (2017).
- [18] D. A. Zezyulin, Y. V. Kartashov, D. V. Skryabin, and I. A. Shelykh, “Spin-orbit coupled polariton condensates in a radially periodic potential: Multiring vortices and rotating solitons,” *ACS Photonics* **5**, 3634 (2018).
- [19] Y. J. Lin, K. Jiménez-García, and I. B. Spielman, “Spin-orbit-coupled Bose-Einstein condensates,” *Nature (London)* **471**, 83 (2011).
- [20] J.-Y. Zhang, S.-C. Ji, Z. Chen, L. Zhang, Z.-D. Du, B. Yan, G.-S. Pan, B. Zhao, Y.-J. Deng, H. Zhai, S. Chen, and J.-W. Pan, “Collective dipole oscillations of a spin-orbit coupled Bose-Einstein condensate,” *Phys. Rev. Lett.* **109**, 115301 (2012).
- [21] S.-C. Ji, L. Zhang, X.-T. Xu, Z. Wu, Y. Deng, S. Chen, and J.-W. Pan, “Softening of roton and phonon modes in a Bose-Einstein condensate with spin-orbit coupling,” *Phys. Rev. Lett.* **114**, 105301 (2015).
- [22] Z. Wu, L. Zhang, W. Sun, X.-T. Xu, B.-Z. Wang, S.-C. Ji, Y. Deng, S. Chen, X.-J. Liu, and J.-W. Pan, “Realization of two-dimensional spin-orbit coupling for Bose-Einstein condensates,” *Science* **354**, 83 (2016).
- [23] F. Dalfovo, S. Giorgini, L. P. Pitaevskii, and S. Stringari, “Theory of Bose-Einstein condensation in trapped gases,” *Rev. Mod. Phys.* **71**, 463 (1999).
- [24] J. Kasprzak, M. Richard, S. Kundermann, A. Baas, P. Jeambrun, J. M. J. Keeling, F. M. Marchetti, M. H. Szymanska, R. André, J. L. Staehli, V. Savona, P. B. Littlewood, B. Deveaud, and L. S. Dang, “Bose-Einstein condensation of exciton polaritons,” *Nature* **443**, 409 (2006).
- [25] R. Balili, V. Hartwell, D. Snoko, L. Pfeiffer, and K. West, “Bose-Einstein condensation of microcavity polaritons in a trap,” *Science* **316**, 1007 (2007).
- [26] S. R. K. Rodriguez, W. Casteels, F. Storme, N. Carlon Zambon, I. Sagnes, L. Le Gratiet, E. Galopin, A. Lemaitre, A. Amo, C. Ciuti, and J. Bloch, “Probing a dissipative phase transition via dynamical optical hysteresis,” *Phys. Rev. Lett.* **118**, 247402 (2017).
- [27] T. Fink, A. Schade, S. Höfling, C. Schneider, and A. Imamoglu, “Signatures of a dissipative phase transition in photon correlation measurements,” *Nature Physics* **14**, 365 (2018).
- [28] S. B. Papp, J. M. Pino, R. J. Wild, S. Ronen, C. E. Wieman, D. S. Jin, and E. A. Cornell, “Bragg spectroscopy of a strongly interacting ^{85}Rb Bose-Einstein condensate,” *Phys. Rev. Lett.* **101**, 135301 (2008).
- [29] S. E. Pollack, D. Dries, M. Junker, Y. P. Chen, T. A. Corcovilos, and R. G. Hulet, “Extreme tunability of interactions in a ^7Li Bose-Einstein condensate,” *Phys. Rev. Lett.* **102**, 090402 (2009).
- [30] N. Navon, S. Piatecki, K. Günter, B. Rem, T. C. Nguyen, F. Chevy, W. Krauth, and C. Salomon, “Dynamics and thermodynamics of the low-temperature strongly interacting Bose gas,” *Phys. Rev. Lett.* **107**, 135301 (2011).
- [31] D. S. Petrov, “Quantum mechanical stabilization of a collapsing Bose-Bose mixture,” *Phys. Rev. Lett.* **115**, 155302 (2015).
- [32] C. R. Cabrera, L. Tanzi, J. Sanz, B. Naylor, P. Thomas, P. Cheiney, and L. Tarruell, “Quantum liquid droplets in a mixture of Bose-Einstein condensates,” *Science* **359**, 301 (2018).
- [33] G. Semeghini, G. Ferioli, L. Masi, C. Mazzinghi, L. Wolswijk, F. Minardi, M. Modugno, G. Modugno, M. Inguscio, and M. Fattori, “Self-bound quantum droplets of atomic mixtures in free space,” *Phys. Rev. Lett.* **120**, 235301 (2018).
- [34] N. B. Jørgensen, G. M. Bruun, and J. J. Arlt, “Dilute fluid governed by quantum fluctuations,” *Phys. Rev. Lett.* **121**, 173403 (2018).
- [35] H. Zhai, “Degenerate quantum gases with spin-orbit coupling: a review,” *Rep. Prog. Phys.* **78**, 026001 (2015).
- [36] T. Ozawa and G. Baym, “Stability of ultracold atomic Bose condensates with Rashba spin-orbit coupling against quantum and thermal fluctuations,” *Phys. Rev. Lett.* **109**, 025301 (2012).
- [37] X. Cui and Q. Zhou, “Enhancement of condensate depletion due to spin-orbit coupling,” *Phys. Rev. A* **87**, 031604(R) (2013).
- [38] W. Zheng, Z.-Q. Yu, X. Cui, and H. Zhai, “Properties of Bose gases with the Raman-induced spin-orbit coupling,” *J. Phys. B* **46**, 134007 (2013).
- [39] E. Kawasaki and M. Holzmann, “Finite-temperature phases of two-dimensional spin-orbit-coupled bosons,” *Phys. Rev. A* **95**, 051601(R) (2017).
- [40] R. Wu and Z. Liang, “Beliaev damping of a spin-orbit-coupled Bose-Einstein condensate,” *Phys. Rev. Lett.* **121**, 180401 (2018).
- [41] Y. Li, L. P. Pitaevskii, and S. Stringari, “Quantum tricriticality and phase transitions in spin-orbit coupled Bose-Einstein condensates,” *Phys. Rev. Lett.* **108**, 225301 (2012).
- [42] Y. Li, G. I. Martone, and S. Stringari, “Sum rules, dipole oscillation and spin polarizability of a spin-orbit coupled quantum gas,” *EPL* **99**, 56008 (2012).
- [43] G. I. Martone, Y. Li, L. P. Pitaevskii, and S. Stringari, “Anisotropic dynamics of a spin-orbit-coupled Bose-Einstein condensate,” *Phys. Rev. A* **86**, 063621 (2012).
- [44] Y.-C. Zhang, Z.-Q. Yu, T. K. Ng, S. Zhang, L. Pitaevskii, and S. Stringari, “Superfluid density of a spin-orbit-coupled Bose gas,” *Phys. Rev. A* **94**, 033635 (2016).
- [45] X.-L. Chen, J. Wang, Y. Li, X.-J. Liu, and H. Hu, “Quantum depletion and superfluid density of a supersolid in Raman spin-orbit-coupled Bose gases,” *Phys. Rev. A* **98**, 013614 (2018).
- [46] P. Wang, Z.-Q. Yu, Z. Fu, J. Miao, L. Huang, S. Chai, H. Zhai, and J. Zhang, “Spin-orbit coupled degenerate Fermi gases,” *Phys. Rev. Lett.* **109**, 095301 (2012).
- [47] L. W. Cheuk, A. T. Sommer, Z. Hadzibabic, T. Yefsah, W. S. Bakr, and M. W. Zwierlein, “Spin-injection spectroscopy of a spin-orbit coupled Fermi gas,” *Phys. Rev. Lett.* **109**, 095302 (2012).
- [48] C. H. L. Quay, T. L. Hughes, J. A. Sulpizio, L. N. Pfeiffer, K. W. Baldwin, K. W. West, D. Goldhaber-Gordon, and R. de Picciotto, “Observation of a one-dimensional spin-orbit gap in a quantum wire,”

- Nature Physics **6**, 336 (2010).
- [49] V. Mourik, K. Zuo, S. M. Frolov, S. R. Plissard, E. P. A. M. Bakkers, and L. P. Kouwenhoven, "Signatures of Majorana fermions in hybrid superconductor-semiconductor nanowire devices," *Science* **336**, 1003 (2012).
- [50] A. Das, Y. Ronen, Y. Most, Y. Oreg, M. Heiblum, and H. Shtrikman, "Zero-bias peaks and splitting in an Al-InAs nanowire topological superconductor as a signature of Majorana fermions," *Nature Physics* **8**, 887 (2012).
- [51] T. D. Lee, K. Huang, and C. N. Yang, "Eigenvalues and eigenfunctions of a Bose system of hard spheres and its low-temperature properties," *Phys. Rev.* **106**, 1135 (1957).
- [52] J. O. Andersen, "Theory of the weakly interacting Bose gas," *Rev. Mod. Phys.* **76**, 599 (2004).
- [53] A. J. Leggett, "On the Superfluid Fraction of an Arbitrary Many-Body System at $T=0$," *J. Stat. Phys.* **93**, 927 (1998).
- [54] X.-L. Chen, X.-J. Liu, and H. Hu, "Quantum and thermal fluctuations in a Raman spin-orbit-coupled Bose gas," *Phys. Rev. A* **96**, 013625 (2017).
- [55] S. T. Beliaev, "Energy-spectrum of a non-ideal Bose gas," *Sov. Phys. JETP* **7**, 299 (1958).
- [56] P. C. Hohenberg and P. C. Martin, "Microscopic theory of superfluid helium," *Ann. Phys. (N. Y.)* **34**, 291 (1965).
- [57] L. P. Pitaevskii and S. Stringari, "Landau damping in dilute Bose gases," *Phys. Lett. A* **235**, 398 (1997).
- [58] W. V. Liu, "Theoretical study of the damping of collective excitations in a Bose-Einstein condensate," *Phys. Rev. Lett.* **79**, 4056 (1997).
- [59] P. O. Fedichev, G. V. Shlyapnikov, and J. T. M. Walraven, "Damping of low-energy excitations of a trapped Bose-Einstein condensate at finite temperatures," *Phys. Rev. Lett.* **80**, 2269 (1998).

Supplemental Material to “Quantum corrections to a spin-orbit coupled Bose-Einstein Condensate”

Long Liang^{1,2} and Päivi Törmä¹

1, Department of Applied Physics, Aalto University School of Science, FI-00076 Aalto, Finland
2, Computational Physics Laboratory, Physics Unit, Faculty of Engineering and Natural Sciences, Tampere University, P.O. Box 692, FI-33014 Tampere, Finland

arXiv:1903.08182v1 [cond-mat.quant-gas] 19 Mar 2019

THEORETICAL FORMALISM

We consider a spin-1/2 Bose gas subjected to a Raman induced spin-orbit coupling [1]. The single-particle Hamiltonian is (we set $\hbar = m = 1$)

$$h_0 = \frac{(p_x - k_0 \sigma_z)^2 + p_y^2 + p_z^2}{2} + \frac{\Omega}{2} \sigma_x, \quad (1)$$

where k_0 is the spin-orbit coupling strength, which is given by the momentum transfer from the two counterpropagating Raman laser beams, σ_i with $i = x, y, z$ are the 2×2 Pauli matrices describing the internal states of the atoms, and Ω is the Rabi frequency of the beams.

The interaction of a spin-1/2 Bose gas is generally written as

$$H_{\text{int}} = \frac{1}{2} \int d^3 \mathbf{r} [g_{\uparrow\uparrow} n_{\uparrow}(\mathbf{r}) n_{\uparrow}(\mathbf{r}) + g_{\uparrow\downarrow} n_{\uparrow}(\mathbf{r}) n_{\downarrow}(\mathbf{r}) + 2g_{\downarrow\downarrow} n_{\downarrow}(\mathbf{r}) n_{\downarrow}(\mathbf{r})], \quad (2)$$

where n_{σ} is the density of particles with spin σ , and $g_{\sigma\sigma'} = 4\pi a_{\sigma\sigma'}$ are the interaction strengths in different spin channels, with $a_{\sigma\sigma'}$ being the corresponding s -wave scattering length. In the following we assume $g_{\uparrow\uparrow} = g_{\downarrow\downarrow} \equiv g$ and $g_{\uparrow\downarrow} \equiv g'$. It is convenient to define interaction parameters $G_1 = g_+ \rho$ and $G_2 = g_- \rho$ with $g_{\pm} = (g \pm g')/2$ and $\rho = N/V$ being the total particle density. The interaction can be rewritten in terms of g_{\pm} as

$$H_{\text{int}} = \frac{1}{2} \int d^3 \mathbf{r} g_+ [n_{\uparrow}(\mathbf{r}) + n_{\downarrow}(\mathbf{r})]^2 + g_- [n_{\uparrow}(\mathbf{r}) - n_{\downarrow}(\mathbf{r})]^2. \quad (3)$$

This model shows three different phases [1, 2], i.e., the stripe, plane wave, and zero momentum phases. We focus on the parameter region $\Omega > 2k_0^2 - 2G_2$, where the condensate is in the zero momentum phase. To study the quantum fluctuations we write the spinor field as

$$\psi = \frac{e^{i\phi}}{\sqrt{2}} \begin{bmatrix} \sqrt{\rho + \zeta_1} e^{i\varphi} \\ -\sqrt{\rho + \zeta_2} e^{-i\varphi} \end{bmatrix}, \quad (4)$$

where ϕ is the total phase and φ is the relative phase of the condensate, and ζ_1 and ζ_2 are the density fluctuations for spin up and spin down particles, respectively. The fluctuations can be parameterized in different manners [3, 4], for example, one can write the real and imaginary part of the fluctuations separately; however, the modulus-phase representation has the advantage that there is no infrared logarithmic divergence in one-loop diagrams and the ultraviolet divergences can be easily removed by adding counter terms [3, 4].

We use the imaginary time path integral formalism. The Euclidean action is given by

$$S = \int_0^{\beta} d\tau \int d^3 x \mathcal{L}, \quad (5)$$

where τ is the imaginary time, $\beta = 1/T$ is the inverse temperature (we take $k_B = 1$), and the Lagrangian density is obtained through the Hamiltonian as

$$\mathcal{L} = \psi^\dagger (\partial_\tau + h_0 - \mu) \psi + \frac{1}{2} [g_+ (\psi^\dagger \psi)^2 + g_- (\psi^\dagger \sigma_z \psi)^2]. \quad (6)$$

We have introduced the chemical potential μ . It is convenient to introduce the density and spin fluctuations, $\zeta_+ = (\zeta_1 + \zeta_2)/2$ and $\zeta_- = (\zeta_1 - \zeta_2)/2$, which are conjugate to ϕ and θ , respectively. We then expand the Lagrangian density in terms of the new variables. Up to the fourth order of the fields, we get

$$\mathcal{L} = \mathcal{L}_{\text{mf}} + \mathcal{L}_{\text{fluct}}, \quad (7)$$

where

$$\mathcal{L}_{\text{mf}} = \left(G_1 + \frac{k_0^2 - \Omega}{2} - \mu \right) \zeta_+ - \mu \rho + \frac{g_+ \rho^2}{2} + \frac{1}{2} [\phi, \zeta_+, \varphi, \zeta_-] \mathcal{G}_0^{-1} [\phi, \zeta_+, \varphi, \zeta_-]^T, \quad (8)$$

is the mean-field Lagrangian density and

$$\begin{aligned} \mathcal{L}_{\text{fluct}} = & \frac{\zeta_+}{2} [(\nabla\phi)^2 + (\nabla\varphi)^2] + \zeta_- \nabla\phi \nabla\varphi - \frac{\Omega\rho}{3} \varphi^4 + \Omega\zeta_+ \varphi^2 - \frac{\Omega}{2\rho} \zeta_-^2 \varphi^2 - \frac{\Omega}{2} \left(\frac{\zeta_+ \zeta_-^2}{2\rho^2} - \frac{\zeta_-^2 \zeta_+^2}{2\rho^3} - \frac{\zeta_-^4}{8\rho^3} \right), \\ & - \frac{\zeta_+ [(\nabla\zeta_+)^2 + (\nabla\zeta_-)^2]}{8\rho^2} - \frac{\zeta_- \nabla\zeta_+ \nabla\zeta_-}{4\rho^2} + \frac{(\zeta_+^2 + \zeta_-^2) [(\nabla\zeta_+)^2 + (\nabla\zeta_-)^2] + \nabla\zeta_+^2 \nabla\zeta_-^2}{8\rho^3}, \end{aligned} \quad (9)$$



FIG. 1. Feynman digrams for diagonal elements of the mean-field Green's function.

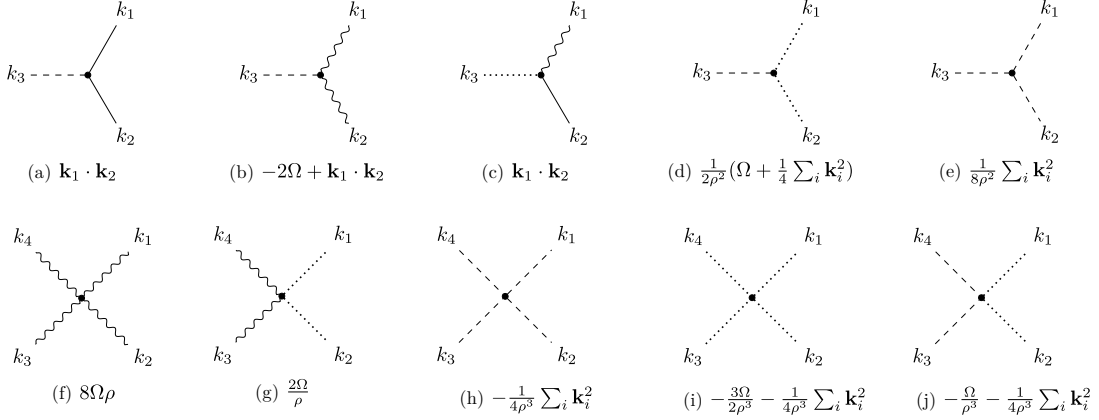


FIG. 2. Feynman diagrams for vertices corresponding to Eq. (9).

describes the beyond mean-field fluctuations. Note that it is necessary to expand the Lagrangian density up to the fourth order of the fields to obtain the full one-loop corrections.

The chemical potential is determined by requiring $\langle \zeta_+ \rangle = 0$, and at the mean-field level this gives $\mu = G_1 + (k_0^2 - \Omega)/2$, so the first order term of the field vanishes and the mean-field Lagrangian density is quadratic, with the mean-field Green's function in the momentum and frequency representation given by

$$\mathcal{G}_0^{-1}(q) = \begin{bmatrix} \mathcal{A}(\mathbf{q}) & -\omega_n & 0 & -ik_0q_x \\ \omega_n & \mathcal{B}(\mathbf{q}) & ik_0q_x & 0 \\ 0 & -ik_0q_x & \mathcal{C}(\mathbf{q}) & -\omega_n \\ ik_0q_x & 0 & \omega_n & \mathcal{D}(\mathbf{q}) \end{bmatrix}, \quad (10)$$

where $q = (i\omega_n, \mathbf{q})$ with $\omega_n = 2\pi n/\beta$ being the Matsubara frequency, $\mathcal{A}(\mathbf{q}) = \rho\mathbf{q}^2$, $\mathcal{B}(\mathbf{q}) = \mathbf{q}^2/(4\rho) + g_+$, $\mathcal{C}(\mathbf{q}) = \rho\mathbf{q}^2 + 2\Omega\rho$, and $\mathcal{D}(\mathbf{q}) = \mathbf{q}^2/(4\rho) + g_- + \Omega/(2\rho)$. The diagonal elements of \mathcal{G}_0 are represented by Feynman diagrams shown in Fig. 1. The vertices corresponding to Eq. (9) are shown in Fig. 2.

MEAN-FIELD RESULTS

In this section we present some mean-field results. The excitation energy is determined by $\det \mathcal{G}_0^{-1} = 0$, which gives

$$\varepsilon_{\text{ph}}^2(\mathbf{q}) = \frac{a(\mathbf{q}) - \sqrt{a^2(\mathbf{q}) - b(\mathbf{q})}}{2}, \quad \varepsilon_{\text{sp}}^2(\mathbf{q}) = \frac{a(\mathbf{q}) + \sqrt{a^2(\mathbf{q}) - b(\mathbf{q})}}{2}, \quad (11)$$

where $a(\mathbf{q}) = \mathcal{A}(\mathbf{q})\mathcal{B}(\mathbf{q}) + \mathcal{C}(\mathbf{q})\mathcal{D}(\mathbf{q}) + 2k_0^2q_x^2$, $b(\mathbf{q}) = 4[\mathcal{A}(\mathbf{q})\mathcal{D}(\mathbf{q}) - k_0^2q_x^2][\mathcal{B}(\mathbf{q})\mathcal{C}(\mathbf{q}) - k_0^2q_x^2]$, ε_{ph} is the gapless phonon mode, and ε_{sp} is the gapped mode which is dominated by spin excitations. In the small momentum limit,

$$\varepsilon_{\text{sp}} = \sqrt{\Omega(\Omega + 2G_2)} + \frac{(G_2 + \Omega)(2G_2 + \Omega) + 2k_0^2(\Omega + G_1 + 2G_2) \cos^2 \theta}{2\sqrt{\Omega}(2G_2 + \Omega)^{3/2}} q^2, \quad (12)$$

$$\varepsilon_{\text{ph}} = c_\theta q + d_\theta q^3, \quad (13)$$

where

$$c_\theta = c_0 \sqrt{1 - \frac{2k_0^2 \cos^2 \theta}{\Omega + 2G_2}}, \quad (14)$$

$$d_\theta = \frac{1}{8c_\theta} \left(1 - \frac{4k_0^2[(\Omega + 2G_2)(\Omega^2 + (G_1 + 3G_2)\Omega + 2(G_1 + G_2)^2) \cos^2 \theta - k_0^2(\Omega + 2(G_1 + G_2))^2 \cos^4 \theta]}{\Omega(\Omega + 2G_2)^3} \right), \quad (15)$$

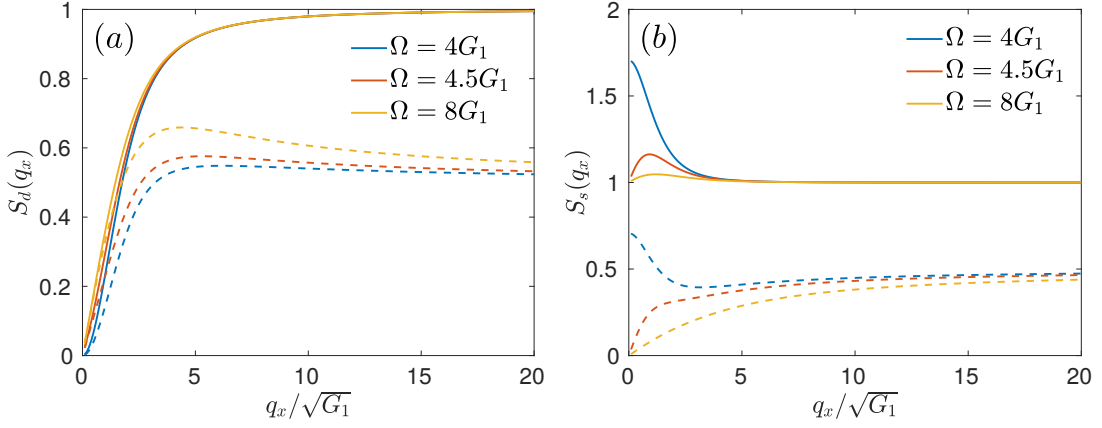


FIG. 3. The density (a) and spin (b) static structure factor. The contribution of the phonon branch are shown by dashed lines. The interaction is taken to be $SU(2)$ invariant, and the spin-orbit coupling is $k_0^2 = 2G_1$.

with $c_0 = \sqrt{G_1}$ being the usual Bogoliubov sound velocity for a weakly interacting single component Bose-Einstein condensate. In the absence of spin-orbit coupling, the sound velocity is the same as c_0 . In the presence of spin-orbit coupling, it depends on θ , which is the angle between the momentum \mathbf{q} and direction of the spin-orbit coupling. When $\Omega = 2k_0^2 - 2G_2$, the sound velocity along the x direction becomes zero, and the phonon dispersion along the x direction becomes quadratic,

$$\varepsilon_{\text{ph}} = \sqrt{G_1 q_{\parallel}^2 + \frac{1}{4} q_{\parallel}^4 + \frac{G_2 q_x^4}{4G_2 + 2\Omega} - \frac{(G_1 + G_2)(2(G_1 + G_2) + \Omega)}{2\Omega(2G_2 + \Omega)} q_{\parallel}^2 q_x^2}, \quad (16)$$

with $q_{\parallel}^2 = q_y^2 + q_z^2$.

Knowing the low energy dispersion relation of the phonons, we can define the momentum region in which the dispersion is linear. When the momentum is along the x direction, by requiring $c_x q_x \gg d_x q_x^3$, we find the condition

$$q_x \ll \sqrt{\Omega - 2k_0^2}. \quad (17)$$

When the momentum is along the y or z direction, the condition is

$$q_y, q_z \ll \sqrt{G_1}. \quad (18)$$

At finite temperature, the linear dispersion region also requires that the dispersion of the thermal excitations is linear, and this leads to the condition

$$T \ll \Omega - 2k_0^2. \quad (19)$$

These conditions are used when deriving the analytical expressions for Beliaev and Landau damping rates.

In the modulus-phase representation, the density and spin response functions are given by the Green's functions $\mathcal{G}_{\zeta_+\zeta_+}$ and $\mathcal{G}_{\zeta_-\zeta_-}$, respectively. So the spin polarizability defined in [5, 6] is simply given by $\mathcal{G}_{\zeta_-\zeta_-}(q_x \rightarrow 0)/\rho$, and at the mean-field level,

$$\chi_M = \mathcal{G}_{0,\zeta_-\zeta_-}(q_x \rightarrow 0)/\rho = \frac{2}{\Omega + 2G_2 - 2k_0^2}. \quad (20)$$

The mean-field density and spin static structure factors can be obtained as

$$S_d(\mathbf{q}) = \int d\omega \mathcal{G}_{0,\zeta_+\zeta_+}(\omega, \mathbf{q})/\rho, \quad S_s(\mathbf{q}) = \int d\omega \mathcal{G}_{0,\zeta_-\zeta_-}(\omega, \mathbf{q})/\rho. \quad (21)$$

We plot the static structure factors in Fig. 3. As comparison, the contributions of the phonon branch are also shown. Without spin-orbit coupling, the density and spin excitations are decoupled and the phonon branch does not contribute to the spin structure factor. In the presence of spin-orbit coupling, a density perturbation along the x direction also induces a spin response and vice versa, so the density and spin structure factors are carried by both the phonon and gapped excitations. Remarkably, we find a peak in the total spin static structure factor. When the parameter

approaches to the phase transition point, the peak becomes higher and its location moves to the zero momentum. By contrast, the peak is not observed in the total density structure factor, although there is peak in the contribution of the phonon branch.

To get the superfluid density, we integrate out the φ and ζ_- fields and obtain an effective theory of ϕ and ζ_+

$$\mathcal{L}_{\text{eff}} = \frac{1}{2}[\phi, \zeta_+] \mathcal{G}_{0,\text{eff}}^{-1} [\phi, \zeta_+]^T, \quad (22)$$

where

$$\mathcal{G}_{0,\text{eff}}^{-1} = \begin{bmatrix} \rho \mathbf{q}^2 & -\omega_n \\ \omega_n & \frac{\mathbf{q}^2}{4\rho} + g_+ \end{bmatrix} - \begin{bmatrix} 0 & ik_0 q_x \\ -ik_0 q_x & 0 \end{bmatrix} \begin{bmatrix} \rho \mathbf{q}^2 + 2\Omega\rho & -\omega_n \\ \omega_n & \frac{\mathbf{q}^2}{4\rho} + g_- + \frac{\Omega}{2\rho} \end{bmatrix}^{-1} \begin{bmatrix} 0 & ik_0 q_x \\ -ik_0 q_x & 0 \end{bmatrix}, \quad (23)$$

which in the low energy limit is

$$\mathcal{G}_{0,\text{eff}}^{-1} = \begin{bmatrix} \rho(\mathbf{q}^2 - \frac{2k_0^2}{\Omega + 2G_2} q_x^2) & -\omega_n \\ \omega_n & \frac{\mathbf{q}^2}{4\rho} + g_+ \end{bmatrix}. \quad (24)$$

Integrating out the ζ_+ field, we arrive at an effective Lagrangian of the phase fluctuation, and in the low energy and long wave length limit,

$$\mathcal{L}_{\text{eff}} = (K^{-1}\omega_n^2 + \rho_i q_i^2) |\phi|^2, \quad (25)$$

where K is the zero momentum static density response function whose mean-field value is $1/g_+$, and the mean-field superfluid densities are

$$\rho_x = \rho \left(1 - \frac{2k_0^2}{\Omega + 2G_2} \right), \quad \rho_y = \rho_z = \rho. \quad (26)$$

ANALYTICAL RESULTS OF ONE-LOOP CORRECTIONS IN THE ABSENCE OF SPIN-ORBIT COUPLING

Without the spin-orbit coupling, we can calculate the one-loop corrections analytically. It is useful to calculate the following integral,

$$I(\alpha, m^2; \beta, M^2; \gamma) = \int \frac{d^d k}{(2\pi)^d} \frac{k^\gamma}{(k^2 + m^2)^\alpha (k^2 + M^2)^\beta} = \frac{2\pi^{d/2}}{(2\pi)^d \Gamma(d/2)} \int dk \frac{k^{d-1+\gamma}}{(k^2 + m^2)^\alpha (k^2 + M^2)^\beta}, \quad (27)$$

$$= \frac{2\pi^{d/2}}{(2\pi)^d \Gamma(d/2)} \int dk \frac{\Gamma(\alpha + \beta)}{\Gamma(\alpha)\Gamma(\beta)} \int_0^1 dx \frac{k^{d-1+\gamma} x^{\alpha-1} (1-x)^{\beta-1}}{[x(k^2 + m^2) + (1-x)(k^2 + M^2)]^{\alpha+\beta}}, \quad (28)$$

$$= \frac{2\pi^{d/2}}{(2\pi)^d \Gamma(d/2)} \frac{(M^2)^{\frac{d+\gamma}{2} - \alpha - \beta}}{\Gamma(\alpha + \beta)} \Gamma\left(\alpha + \beta - \frac{d + \gamma}{2}\right) \Gamma\left(\frac{d + \gamma}{2}\right) {}_2F_1\left(\alpha, \alpha + \beta - \frac{d + \gamma}{2}; \alpha + \beta; 1 - \frac{m^2}{M^2}\right), \quad (29)$$

where ${}_2F_1(a, b; c; z)$ is the hypergeometric function. To get the above result we have used dimensional regularization.

The condensate fraction is

$$|\langle \psi_\uparrow \rangle|^2 + |\langle \psi_\downarrow \rangle|^2 = \frac{1}{2} \left(|\langle \sqrt{\rho + \zeta_1} e^{i(\phi + \varphi)} \rangle|^2 + |\langle -\sqrt{\rho + \zeta_2} e^{i(\phi - \varphi)} \rangle|^2 \right), \quad (30)$$

$$\approx \rho - \frac{1}{4\rho} (\langle \zeta_+^2 \rangle + \langle \zeta_-^2 \rangle) - \rho (\langle \varphi^2 \rangle + \langle \phi^2 \rangle), \quad (31)$$

so the quantum depletion is

$$\delta\rho = \frac{1}{4\rho} (\langle \zeta_+^2 \rangle + \langle \zeta_-^2 \rangle) + \rho (\langle \varphi^2 \rangle + \langle \phi^2 \rangle), \quad (32)$$

$$= \frac{(g_+ \rho)^{3/2}}{3\pi^2} + \frac{(g_- \rho)^{3/2}}{3\pi^2} \sqrt{1 + x/2} \left[(x + 1)E\left(\frac{2}{x + 2}\right) - xK\left(\frac{2}{x + 2}\right) \right], \quad (33)$$

with $x = \Omega/(g_- \rho)$ and $E(z)$ and $K(z)$ are the complete elliptic integral of the second and first kind, respectively. The quantum depletion increases with increasing g_+ and g_- , but decreases with increasing Ω .

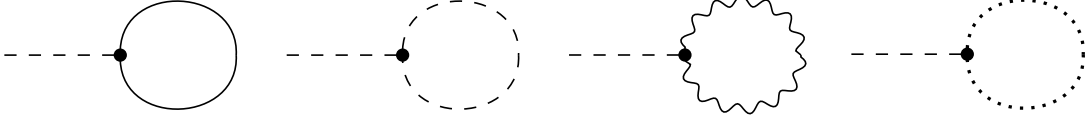


FIG. 4. Feynman diagrams that determine the chemical potential shift $\delta\mu$. These tadpole diagrams are canceled by the chemical potential shift and therefore do not contribute to the one-loop self-energy. For notation see Fig. 1.

The transverse spin polarization is

$$\langle\sigma_x\rangle = \frac{1}{\rho}\langle\psi^\dagger\sigma_x\psi\rangle \approx -1 + 2\langle\varphi^2\rangle + \frac{1}{2\rho^2}\langle\zeta_-^2\rangle, \quad (34)$$

so

$$\delta\langle\sigma_x\rangle = 2\langle\varphi^2\rangle + \frac{1}{2\rho^2}\langle\zeta_-^2\rangle, \quad (35)$$

$$= \frac{2(g_-\rho)^{3/2}}{3\rho\pi^2}\sqrt{1+x/2}\left[(x+1)E\left(\frac{2}{x+2}\right) - xK\left(\frac{2}{x+2}\right)\right]. \quad (36)$$

The Lee-Huang-Yang correction [7] can be obtained as the zero point energy of the system [4], and we find

$$\mathcal{E}_{\text{LHY}} = \frac{8}{15\pi^2}g_+\rho^2\sqrt{g_+^3\rho} + \frac{(g_-\rho)^{5/2}\sqrt{1+x/2}}{4\pi}{}_2F_1\left(-\frac{1}{2}, \frac{3}{2}; 3; \frac{2}{2+x}\right). \quad (37)$$

The first term in Eq. (37) is the same as the result for a weakly-interacting spinless Bose gas [7]. The second term comes from the spin excitation. The function ${}_2F_1\left(-\frac{1}{2}, \frac{3}{2}; 3; \frac{2}{2+x}\right)$ depends weakly on x , with ${}_2F_1\left(-\frac{1}{2}, \frac{3}{2}; 3; 1\right) = 32/(15\pi)$ and ${}_2F_1\left(-\frac{1}{2}, \frac{3}{2}; 3; 0\right) = 1$, so the second term increases with increasing g_- and Ω .

The chemical potential shift is given by the tadpole diagrams shown in Fig. 4. Evaluating the integrals, we find

$$\delta\mu = \frac{4g_+\rho\sqrt{g_+^3\rho}}{3\pi^2} + \frac{g_-\rho\sqrt{g_-^3\rho}\sqrt{1+x/2}}{3\pi^2}\left[(4+x)E\left(\frac{2}{2+x}\right) - xK\left(\frac{2}{2+x}\right)\right], \quad (38)$$

which increases with g_+ , g_- , and Ω . Another way to calculate the chemical potential shift is to take derivative of the LHY energy density \mathcal{E}_{LHY} with respect to ρ , $\delta\mu = \partial_\rho\mathcal{E}_{\text{LHY}}$, and the result is the same as Eq. (38).

The correction to K^{-1} is given by $\Sigma_{\zeta_+\zeta_+}(0)$, and in the absence of spin-orbit coupling,

$$\delta K^{-1} = -\Sigma_{\zeta_+\zeta_+}(0) = \frac{2g_+\sqrt{g_+^3\rho}}{\pi^2} + \frac{g_-\sqrt{g_-^3\rho}\sqrt{1+x/2}}{2\pi}{}_2F_1\left(-\frac{1}{2}, -\frac{1}{2}; 1; \frac{2}{2+x}\right). \quad (39)$$

Note that δK^{-1} can be related to $\delta\mu$ through $\delta K^{-1} = \partial_\rho\delta\mu$.

To calculate the correction to the mean-field excitation gap Δ_0 , we need to compute the self-energies $\Sigma_{\varphi\varphi}(\Delta_0)$, $\Sigma_{\zeta_-\zeta_-}(\Delta_0)$, and $\Sigma_{\varphi\zeta_-}(\Delta_0)$, which can also be done analytically in the absence of the spin-orbit coupling, and we find that the one-loop correction to the gap is zero. In the presence of spin-orbit coupling, we calculate the self-energies numerically, and find the one-loop correction increases the gap slightly, see the main paper.

THE DAMPING RATE AT ZERO AND FINITE TEMPERATURE

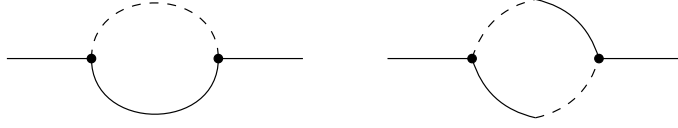
In this section we calculate the damping rate γ , which is the imaginary part of the phonon excitation energy. We calculate the damping rate by solving

$$\det[G_0^{-1}(\varepsilon_{\text{ph}} - i\gamma, \mathbf{q}) - \Sigma(\varepsilon_{\text{ph}} + i0^+, \mathbf{q})] = 0, \quad (40)$$

where $\Sigma(\varepsilon_{\text{ph}} + i0^+, \mathbf{q})$ is the one-loop self-energy evaluated at the phonon frequency.

To solve Eq. (40), we first integrate out the φ and ζ_- fields and obtain an effective theory for the low energy mode [c.f. Eq. (22)]

$$\mathcal{L}_{\text{eff}} = \frac{1}{2}[\phi, \zeta_+]\mathcal{G}_{\text{eff}}^{-1}[\phi, \zeta_+]^T, \quad (41)$$

FIG. 5. Feynman diagrams for $\Sigma_{\phi\phi}$.

where

$$\mathcal{G}_{\text{eff}}^{-1} = \begin{bmatrix} \rho(\mathbf{q}^2 - \frac{2k_0^2}{\Omega+2G_2}q_x^2) & -\omega_n \\ \omega_n & \frac{\mathbf{q}^2}{4\rho} + g_+ \end{bmatrix} - \begin{bmatrix} \Sigma_{\text{eff},\phi\phi} & \Sigma_{\text{eff},\phi\zeta_+} \\ \Sigma_{\text{eff},\zeta_+\phi} & \Sigma_{\text{eff},\zeta_+\zeta_+} \end{bmatrix}. \quad (42)$$

And then from Eq. (42), the damping rate is obtained

$$\gamma = \frac{\rho(\mathbf{q}^2 - \frac{2k_0^2}{\Omega+2G_2}q_x^2)\Im\Sigma_{\text{eff},\zeta_+\zeta_+} + g_+\Im\Sigma_{\text{eff},\phi\phi}}{2\varepsilon_{\text{ph}}} + \Re\Sigma_{\text{eff},\phi\zeta_+}. \quad (43)$$

We focus on the linear dispersion regime defined previously. By analyzing the low energy and momentum behavior of all the one-loop diagrams, we find it is enough to consider the Feynman diagrams constructed from only two vertices Figs. 2 (a) and (d), and the momentum dependence of vertex Fig. 2 (d) can be neglected. Therefore the relevant parts of the effective self-energy matrix is

$$\begin{bmatrix} \Im\Sigma_{\text{eff},\phi\phi} & \Re\Sigma_{\text{eff},\phi\zeta_+} \\ \Re\Sigma_{\text{eff},\zeta_+\phi} & \Im\Sigma_{\text{eff},\zeta_+\zeta_+} \end{bmatrix} = \begin{bmatrix} \Im\Sigma_{\phi\phi} & \Re\Sigma_{\phi\zeta_+} \\ \Re\Sigma_{\zeta_+\phi} & \Im\Sigma_{\zeta_+\zeta_+} \end{bmatrix} + \begin{bmatrix} \frac{4\rho k_0 q_x \Re\Sigma_{\phi\zeta_-} + 4\rho^2 k_0^2 q_x^2 \Re\Sigma_{\zeta_-\zeta_-}}{\Omega+2G_2} + \frac{2\rho k_0 q_x \Im\Sigma_{\zeta_+\zeta_-}}{\Omega+2G_2} & \frac{2\rho k_0 q_x \Im\Sigma_{\zeta_+\zeta_-}}{\Omega+2G_2} \\ -\frac{2\rho k_0 q_x \Im\Sigma_{\zeta_+\zeta_-}}{\Omega+2G_2} & 0 \end{bmatrix}. \quad (44)$$

As an example, we calculate $\Sigma_{\phi\phi}(i\omega_n, \mathbf{q})$ explicitly. The Feynman diagrams are shown in Fig. 5.

$$\begin{aligned} \Sigma_{\phi\phi}(i\omega_n, \mathbf{q}) = \sum_{\omega'_m, \mathbf{k}} & \left[(\mathbf{k} \cdot \mathbf{q})^2 \mathcal{G}_{0,\phi\phi}(i\omega'_m, \mathbf{k}) \mathcal{G}_{0,\sigma_+\sigma_+}(i\omega_n - i\omega'_m, \mathbf{q} - \mathbf{k}) \right. \\ & \left. + \mathbf{k} \cdot \mathbf{q}(\mathbf{q}^2 - \mathbf{k} \cdot \mathbf{q}) \mathcal{G}_{0,\phi\sigma_+}(i\omega'_m, \mathbf{k}) \mathcal{G}_{0,\phi\sigma_+}(i\omega_n - i\omega'_m, \mathbf{q} - \mathbf{k}) \right]. \end{aligned} \quad (45)$$

We write the noninteracting Green's function explicitly

$$\mathcal{G}_{0,\phi\phi}(i\omega_n, \mathbf{q}) = \frac{A_{11}(\mathbf{q})}{\omega_n^2 + \varepsilon_{\text{sp}}^2(\mathbf{q})} + \frac{B_{11}(\mathbf{q})}{\omega_n^2 + \varepsilon_{\text{ph}}^2(\mathbf{q})}, \quad (46)$$

$$\mathcal{G}_{0,\zeta_+\zeta_+}(i\omega_n, \mathbf{q}) = \frac{A_{22}(\mathbf{q})}{\omega_n^2 + \varepsilon_{\text{sp}}^2(\mathbf{q})} + \frac{B_{22}(\mathbf{q})}{\omega_n^2 + \varepsilon_{\text{ph}}^2(\mathbf{q})}, \quad (47)$$

$$\mathcal{G}_{0,\phi\zeta_+}(i\omega_n, \mathbf{q}) = -\mathcal{G}_{0,\zeta_+\phi}(i\omega_n, \mathbf{q}) = \frac{\omega A_{12}(\mathbf{q})}{\omega_n^2 + \varepsilon_{\text{sp}}^2(\mathbf{q})} + \frac{\omega B_{12}(\mathbf{q})}{\omega_n^2 + \varepsilon_{\text{ph}}^2(\mathbf{q})}. \quad (48)$$

Since we are studying the damping rate in the linear regime, the gapped branch can be neglected, and it is enough to know the low momentum behavior of B_{11} , B_{22} , and B_{12} ,

$$B_{11}(\mathbf{q}) \approx g_+, \quad B_{22}(\mathbf{q}) \approx \rho \frac{c_{\theta}^2}{c_0^2} \mathbf{q}^2, \quad B_{12}(\mathbf{q}) \approx 1. \quad (49)$$

Evaluating the Matsubara frequency summation, $\Sigma_{\phi\phi}(i\omega_n, \mathbf{q})$ can be written as

$$\Sigma_{\phi\phi}(i\omega_n, \mathbf{q}) = \Sigma_{\phi\phi,1}(i\omega_n, \mathbf{q}) + \Sigma_{\phi\phi,2}(i\omega_n, \mathbf{q}), \quad (50)$$

with

$$\begin{aligned} \Sigma_{\phi\phi,1}(i\omega_n, \mathbf{q}) = \sum_{\mathbf{k}} & [1 + n(\varepsilon_{\text{ph}}(\mathbf{k})) + n(\varepsilon_{\text{ph}}(\mathbf{q} - \mathbf{k}))] \left[\frac{1}{-i\omega_n + \varepsilon_{\text{ph}}(\mathbf{k}) + \varepsilon_{\text{ph}}(\mathbf{q} - \mathbf{k})} + \frac{1}{i\omega_n + \varepsilon_{\text{ph}}(\mathbf{k}) + \varepsilon_{\text{ph}}(\mathbf{q} - \mathbf{k})} \right] \\ & \left[(\mathbf{k} \cdot \mathbf{q})^2 \frac{B_{11}(\mathbf{k})B_{22}(\mathbf{q} - \mathbf{k})}{4\varepsilon_{\text{ph}}(\mathbf{k})\varepsilon_{\text{ph}}(\mathbf{q} - \mathbf{k})} + \mathbf{k} \cdot \mathbf{q}(\mathbf{q}^2 - \mathbf{k} \cdot \mathbf{q}) \frac{B_{12}(\mathbf{k})B_{12}(\mathbf{q} - \mathbf{k})}{4} \right], \end{aligned} \quad (51)$$

which is nonzero even if the temperature is zero and is relevant to the Beliaev damping rate, and

$$\begin{aligned} \Sigma_{\phi\phi,2}(i\omega_n, \mathbf{q}) = \sum_{\mathbf{k}} [n(\varepsilon_{\text{ph}}(\mathbf{k})) - n(\varepsilon_{\text{ph}}(\mathbf{q} - \mathbf{k}))] & \left[\frac{1}{i\omega_n + \varepsilon_{\text{ph}}(\mathbf{q} - \mathbf{k}) - \varepsilon_{\text{ph}}(\mathbf{k})} - \frac{1}{i\omega_n + \varepsilon_{\text{ph}}(\mathbf{k}) - \varepsilon_{\text{ph}}(\mathbf{q} - \mathbf{k})} \right] \\ & \left[(\mathbf{k} \cdot \mathbf{q})^2 \frac{B_{11}(\mathbf{k})B_{22}(\mathbf{q} - \mathbf{k})}{4\varepsilon_{\text{ph}}(\mathbf{k})\varepsilon_{\text{ph}}(\mathbf{q} - \mathbf{k})} - \mathbf{k} \cdot \mathbf{q}(\mathbf{q}^2 - \mathbf{k} \cdot \mathbf{q}) \frac{B_{12}(\mathbf{k})B_{12}(\mathbf{q} - \mathbf{k})}{4} \right], \end{aligned} \quad (52)$$

which is nonzero only at finite temperature and is relevant to the Landau damping rate.

We calculate the imaginary part of $\Sigma_{\phi\phi,1}(\varepsilon_{\text{ph}}(\mathbf{q}) + i0^+, \mathbf{q})$ at zero temperature,

$$\Im\Sigma_{\phi\phi,1}(\varepsilon_{\text{ph}}(\mathbf{q}) + i0^+, \mathbf{q}) = \pi \sum_{\mathbf{k}} \delta(-\varepsilon_{\text{ph}}(\mathbf{q}) + \varepsilon_{\text{ph}}(\mathbf{k}) + \varepsilon_{\text{ph}}(\mathbf{q} - \mathbf{k})) f(\mathbf{q}, \mathbf{k}), \quad (53)$$

$$f(\mathbf{q}, \mathbf{k}) = (\mathbf{k} \cdot \mathbf{q})^2 \frac{B_{11}(\mathbf{k})B_{22}(\mathbf{q} - \mathbf{k})}{4\varepsilon_{\text{ph}}(\mathbf{k})\varepsilon_{\text{ph}}(\mathbf{q} - \mathbf{k})} + \mathbf{k} \cdot \mathbf{q}(\mathbf{q}^2 - \mathbf{k} \cdot \mathbf{q}) \frac{B_{12}(\mathbf{k})B_{12}(\mathbf{q} - \mathbf{k})}{4}. \quad (54)$$

To calculate the above integral, we need to solve the internal \mathbf{k} allowed by the energy and momentum conservation. We can scale the momentum as $c_x k_x \equiv c_0 k'_x$ and $k_{y/z} = k'_{y/z}$, and then the phonon dispersion can be written as

$$\varepsilon_{\text{ph}}(\mathbf{k}) = \sqrt{c_x^2 k_x^2 + c_0 k_y^2 + c_0^2 k_z^2} = c_\theta k = c_0 k'. \quad (55)$$

The momentum and energy conservation can be solved in terms of the new variables in the small \mathbf{q} limit (θ' is the angle between \mathbf{k}' and \mathbf{q}'),

$$\delta(-c_0 q' + c_0 k' + c_0 |\mathbf{q}' - \mathbf{k}'|) = \frac{q' - k'}{c_0 q' k' \sin \theta'} \delta(\theta'), \quad (56)$$

with the restriction $k' < q'$. This means that \mathbf{k}' and \mathbf{q}' are along the same direction and $k' < q'$ and therefore \mathbf{k} and \mathbf{q} are also along the same direction and $k < q$. Under this condition,

$$f(\mathbf{q}, \mathbf{k}) = \frac{kq^2(q - k)}{2}, \quad (57)$$

so

$$\Im\Sigma_{\phi\phi,1}(\varepsilon_{\text{ph}}(\mathbf{q}) + i0^+, \mathbf{q}) = \pi \int \frac{dk_x dk_y dk_z}{(2\pi)^3} f(\mathbf{q}, \mathbf{k}) \delta(-\varepsilon_{\text{ph}}(\mathbf{q}) + \varepsilon_{\text{ph}}(\mathbf{k}) + \varepsilon_{\text{ph}}(\mathbf{q} - \mathbf{k})), \quad (58)$$

$$= \pi \frac{c_0}{c_x} \int \frac{dk'_x dk'_y dk'_z}{(2\pi)^3} f(\mathbf{q}, \mathbf{k}) \delta(-c_0 q' + c_0 k' + c_0 |\mathbf{q}' - \mathbf{k}'|), \quad (59)$$

$$= \pi \frac{c_0}{c_x} \int \frac{dk'_x dk'_y dk'_z}{(2\pi)^3} f(q, k) \frac{q' - k'}{c_0 q' k' \sin \theta'} \delta(\theta'), \quad (60)$$

$$= \pi \frac{1}{c_x} \int \frac{k'^2 dk'}{4\pi^2} f(q, k) \frac{q' - k'}{q' k'}, \quad (61)$$

$$= \frac{c_\theta^2}{c_0^2 c_x} \int_0^q \frac{k^2 dk}{4\pi} \frac{kq^2(q - k)}{2} \frac{q - k}{qk}, \quad (62)$$

$$= \frac{1}{2} \frac{c_\theta^2}{c_0^2 c_x} \frac{q^6}{120\pi}. \quad (63)$$

We now calculate $\Im\Sigma_{\phi\phi,2}(\varepsilon_{\text{ph}}(\mathbf{q}) + i0^+, \mathbf{q})$ at finite temperature,

$$\begin{aligned} \Im\Sigma_{\phi\phi,2}(\varepsilon_{\text{ph}}(\mathbf{q}) + i0^+, \mathbf{q}) = \pi \sum_{\mathbf{k}} [n(\varepsilon_{\text{ph}}(\mathbf{k})) - n(\varepsilon_{\text{ph}}(\mathbf{q} - \mathbf{k}))] & \left[(\mathbf{k} \cdot \mathbf{q})^2 \frac{B_{11}(\mathbf{k})B_{22}(\mathbf{q} - \mathbf{k})}{4\varepsilon_{\text{ph}}(\mathbf{k})\varepsilon_{\text{ph}}(\mathbf{q} - \mathbf{k})} - \mathbf{k} \cdot \mathbf{q}(\mathbf{q}^2 - \mathbf{k} \cdot \mathbf{q}) \frac{B_{12}(\mathbf{k})B_{12}(\mathbf{q} - \mathbf{k})}{4} \right] \\ & [-\delta(\varepsilon_{\text{ph}}(\mathbf{q}) + \varepsilon_{\text{ph}}(\mathbf{q} - \mathbf{k}) - \varepsilon_{\text{ph}}(\mathbf{k})) + \delta(\varepsilon_{\text{ph}}(\mathbf{q}) + \varepsilon_{\text{ph}}(\mathbf{k}) - \varepsilon_{\text{ph}}(\mathbf{q} - \mathbf{k}))], \end{aligned} \quad (64)$$

$$= -\pi \sum_{\mathbf{k}} [n(\varepsilon_{\text{ph}}(\mathbf{k} + \mathbf{q})) - n(\varepsilon_{\text{ph}}(\mathbf{k}))] \delta(\varepsilon_{\text{ph}}(\mathbf{q}) + \varepsilon_{\text{ph}}(\mathbf{k}) - \varepsilon_{\text{ph}}(\mathbf{k} + \mathbf{q})) g(\mathbf{q}, \mathbf{k}), \quad (65)$$

$$= -\pi \sum_{\mathbf{k}} \frac{\partial n(\varepsilon_{\text{ph}}(\mathbf{k}))}{\partial \varepsilon_{\text{ph}}(\mathbf{k})} \varepsilon_{\text{ph}}(\mathbf{q}) \delta(\varepsilon_{\text{ph}}(\mathbf{q}) + \varepsilon_{\text{ph}}(\mathbf{k}) - \varepsilon_{\text{ph}}(\mathbf{k} + \mathbf{q})) g(\mathbf{q}, \mathbf{k}), \quad (66)$$

where

$$g(\mathbf{q}, \mathbf{k}) = \left[(\mathbf{k} \cdot \mathbf{q} + \mathbf{q}^2)^2 \frac{B_{11}(\mathbf{k} + \mathbf{q})B_{22}(\mathbf{k})}{4\varepsilon_{\text{ph}}(\mathbf{k} + \mathbf{q})\varepsilon_{\text{ph}}(\mathbf{k})} + (\mathbf{k} \cdot \mathbf{q} + \mathbf{q}^2)\mathbf{k} \cdot \mathbf{q} \frac{B_{12}(\mathbf{k} + \mathbf{q})B_{12}(\mathbf{k})}{2} + (\mathbf{k} \cdot \mathbf{q})^2 \frac{B_{11}(\mathbf{k})B_{22}(\mathbf{q} + \mathbf{k})}{4\varepsilon_{\text{ph}}(\mathbf{k})\varepsilon_{\text{ph}}(\mathbf{q} + \mathbf{k})} \right]. \quad (67)$$

To get Eq. (66) we have assumed $c_\theta q/T \ll 1$ and expand $n(\varepsilon_{\text{ph}}(\mathbf{k} + \mathbf{q})) - n(\varepsilon_{\text{ph}}(\mathbf{k}))$ to the lowest order. In general it is difficult to solve the energy and momentum conserving condition $\delta(\varepsilon_{\text{ph}}(\mathbf{q}) + \varepsilon_{\text{ph}}(\mathbf{k}) - \varepsilon_{\text{ph}}(\mathbf{k} + \mathbf{q}))$ even if \mathbf{q} is small, because \mathbf{k} is not necessarily small and for general \mathbf{k} , the phonon dispersion is very complicated. However, if we focus on the low temperature region such that the corresponding phonon dispersion is linear, then we can replace $\varepsilon_{\text{ph}}(\mathbf{k})$ by the linear dispersion because $\frac{\partial n(\varepsilon_{\text{ph}}(\mathbf{k}))}{\partial \varepsilon_{\text{ph}}(\mathbf{k})}$ decays rapidly when $\varepsilon_{\text{ph}}(\mathbf{k}) > T$. In this region the momentum and energy conservation is easily solved: \mathbf{k} and \mathbf{q} are along the same direction and the length of \mathbf{k} is unrestricted. Under this condition $g(\mathbf{q}, \mathbf{k})$ also takes a simple form

$$g(\mathbf{q}, \mathbf{k}) = kq^2(k + q), \quad (68)$$

and

$$\Im \Sigma_{\phi\phi,2}(\varepsilon_{\text{ph}}(\mathbf{q}) + i0^+, \mathbf{q}) = \frac{c_\theta^2}{c_0^2 c_x} \int_0^\infty \frac{k^2 dk}{4\pi} \frac{\beta e^{\beta c_\theta k}}{(e^{\beta c_\theta k} - 1)^2} c_\theta q k q^2 (k + q) \frac{q + k}{qk}, \quad (69)$$

$$= \frac{q^2 T^4}{c_\theta^2 c_0^2 c_x} \int_0^\infty \frac{x^2 dx}{4\pi} \frac{e^x}{(e^x - 1)^2} \left(x + \frac{c_\theta q}{T}\right)^2, \quad (70)$$

$$= \frac{\pi^3 q^2 T^4}{15 c_\theta^2 c_0^2 c_x}. \quad (71)$$

To get Eq. (71) from Eq. (70), we have used the condition $c_\theta q/T \ll 1$.

We can calculate other self-energies in the similar way, and here we just summarize the final results,

$$\begin{array}{l} \Im \Sigma_{\phi\phi,1} = \frac{1}{2} \frac{c_\theta^2}{c_0^2 c_x} \frac{q^6}{120\pi} \\ \Re \Sigma_{\phi\zeta_{+,1}} = \frac{g_+}{4} \left[1 - \frac{2k_0^2 \Omega \cos^2 \theta}{(\Omega + 2G_2)^2} \right] \frac{c_\theta}{c_0^2 c_x} \frac{q^5}{120\pi} \\ \Im \Sigma_{\zeta_+\zeta_{+,1}} = \frac{g_+}{8\rho} \left[1 - \frac{2\Omega k_0^2 \cos^2 \theta}{(\Omega + 2G_2)^2} \right]^2 \frac{1}{c_x} \frac{q^4}{120\pi} \\ \Im \Sigma_{\zeta_-\zeta_{-,1}} = \frac{k_0^2 \Omega^2 \cos^2 \theta}{2\rho^2 (\Omega + 2G_2)^2} \frac{c_\theta^2}{c_0^2 c_x} \frac{q^4}{120\pi} \\ \Re \Sigma_{\phi\zeta_{-,1}} = \frac{\Omega k_0 \cos \theta}{2\rho(\Omega + 2G_2)} \frac{c_\theta^2}{c_0^2 c_x} \frac{q^5}{120\pi} \\ \Im \Sigma_{\zeta_+\zeta_{-,1}} = \frac{g_+ \Omega k_0 \cos \theta}{4\rho(\Omega + 2G_2)} \left[1 - \frac{2k_0^2 \Omega \cos^2 \theta}{(\Omega + 2G_2)^2} \right] \frac{c_\theta}{c_0^2 c_x} \frac{q^4}{120\pi} \end{array} \left| \begin{array}{l} \Im \Sigma_{\phi\phi,2} = \frac{\pi^3 q^2 T^4}{15 c_\theta^2 c_0^2 c_x} \\ \Re \Sigma_{\phi\zeta_{+,2}} = \frac{g_+}{2} \left[1 - \frac{2k_0^2 \Omega \cos^2 \theta}{(\Omega + 2G_2)^2} \right] \frac{1}{c_0^2 c_\theta^3 c_x} \frac{\pi^3 q T^4}{15} \\ \Im \Sigma_{\zeta_+\zeta_{+,2}} = \frac{g_+}{4\rho} \left[1 - \frac{2\Omega k_0^2 \cos^2 \theta}{(\Omega + 2G_2)^2} \right]^2 \frac{1}{c_\theta^4 c_x} \frac{\pi^3 T^4}{15} \\ \Im \Sigma_{\zeta_-\zeta_{-,2}} = \frac{k_0^2 \Omega^2 \cos^2 \theta}{\rho^2 (\Omega + 2G_2)^2} \frac{1}{c_0^2 c_\theta^3 c_x} \frac{\pi^3 T^4}{15} \\ \Re \Sigma_{\phi\zeta_{-,2}} = \frac{\Omega k_0 \cos \theta}{\rho(\Omega + 2G_2)} \frac{1}{c_0^2 c_\theta^2 c_x} \frac{\pi^3 q T^4}{15} \\ \Im \Sigma_{\zeta_+\zeta_{-,2}} = \frac{g_+ \Omega k_0 \cos \theta}{2\rho(\Omega + 2G_2)} \left[1 - \frac{2k_0^2 \Omega \cos^2 \theta}{(\Omega + 2G_2)^2} \right] \frac{1}{c_0^2 c_\theta^3 c_x} \frac{\pi^3 T^4}{15} \end{array} \right. \quad (72)$$

From the above results we get the Beliaev damping rate at zero temperature

$$\gamma_B = \frac{3g_+ q^5}{640\pi c_\theta} \left[1 - \frac{2\Omega k_0^2 \cos^2 \theta}{(\Omega + 2G_2)^2} \right]^2 \frac{c_\theta^2}{c_0^2 c_x}, \quad (73)$$

$$= \frac{3q^5}{640\pi\rho} \left[1 - \frac{2\Omega k_0^2 \cos^2 \theta}{(\Omega + 2G_2)^2} \right]^2 \frac{c_\theta}{c_x}, \quad (74)$$

$$= \frac{3q^5}{640\pi\rho} \left[1 - \frac{2\Omega k_0^2 \cos^2 \theta}{(\Omega + 2G_2)^2} \right]^2 \sqrt{1 + \frac{2k_0^2 \sin^2 \theta}{\Omega + 2G_2 - 2k_0^2}}. \quad (75)$$

and the Landau damping rate at finite temperature

$$\gamma_L = \frac{3\pi^3 q T^4}{40\rho c_\theta^4} \left[1 - \frac{2\Omega k_0^2 \cos^2 \theta}{(\Omega + 2G_2)^2} \right]^2 \sqrt{1 + \frac{2k_0^2 \sin^2 \theta}{\Omega + 2G_2 - 2k_0^2}}. \quad (76)$$

The Beliaev damping rate takes the same form as the result in [8], where a different method was used. The analytical expression for the Landau damping rate is obtained here for the first time.

If $G_2 = g_{-\rho} = 0$, the damping rates can be further simplified as

$$\gamma_B = \frac{3q^5}{640\pi\rho} \frac{c_\theta^4}{c_0^4} \sqrt{1 + \frac{2k_0^2 \sin^2 \theta}{\Omega - 2k_0^2}}, \quad (77)$$

$$\gamma_L = \frac{3\pi^3 q T^4}{40\rho c_0^4} \sqrt{1 + \frac{2k_0^2 \sin^2 \theta}{\Omega - 2k_0^2}}. \quad (78)$$

Since $c_\theta = c_0 \sqrt{1 - \frac{2k_0^2 \cos^2 \theta}{\Omega + 2G_2}}$, the Beliaev damping is strongly suppressed when the momentum is along the direction of the spin-orbit coupling. However, the Landau damping is not suppressed.

-
- [1] Y. J. Lin, K. Jiménez-García, and I. B. Spielman, *Nature (London)* **471**, 83 (2011).
 - [2] Y. Li, L. P. Pitaevskii, and S. Stringari, *Phys. Rev. Lett.* **108**, 225301 (2012).
 - [3] E. Braaten and A. Nieto, *Phys. Rev. B* **56**, 14745 (1997).
 - [4] J. O. Andersen, *Rev. Mod. Phys.* **76**, 599 (2004).
 - [5] G. I. Martone, Y. Li, L. P. Pitaevskii, and S. Stringari, *Phys. Rev. A* **86**, 063621 (2012).
 - [6] Y. Li, G. I. Martone, and S. Stringari, *EPL* **99**, 56008 (2012).
 - [7] T. D. Lee, K. Huang, and C. N. Yang, *Phys. Rev.* **106**, 1135 (1957).
 - [8] R. Wu and Z. Liang, *Phys. Rev. Lett.* **121**, 180401 (2018).